12TH INTERNATIONAL SYMPOSIUM ON FLOW VISUALIZATION
September 10-14, 2006, German Aerospace Center (DLR), Göttingen, Germany

COMPUTATIONAL VISUALIZATION OF EDDY STRUCTURES AFTER DNS OF FLOW OVER A CYLINDER, OVER A CAVITY AND IN AN ENCLOSURE

V. Goryachev*, A. Abramov, E. Smirnov****
*** Department of Mathematics, Tver State Technical University**
A. Nikitina, 22, Tver, Russia, 170026
**** Department of Aerodynamics**
Saint-Petersburg State Polytechnic University
Polytechnicheskaya Str., 29, Saint-Petersburg, 195251, Russia
Keywords: *DNS, eddy structure, CFD visualization*

ABSTRACT

The report covers modeling of turbulent flows, eddy structure analysis and application of up-to-date visualization techniques to process results of 3D numerical simulation of several fluid dynamics generic cases: unsteady flow over a heated circular cylinder, strongly turbulent Rayleigh-Bénard (RB) convection in a confined enclosure of cubic form, and flow in opened-from-above periodically-placed ventilated cavities. The computations were performed with the Direct Numerical Simulation (DNS) approach. Field data after numerical computations were processed using different visualization tools. Such specific flow features as large-scale circulation and turbulent plumes in the cubic cell, eddies and heated trails inside and downstream of the opened-from-above cavity, vortices behind the cylinder were indicated using visualization techniques accentuated by general flow structure.

1 INTRODUCTION

The present contribution is aimed at eddy structure analysis and practice of postcomputational visualization of results after numerical simulation of turbulent flow over a heated circular cylinder, strongly turbulent Rayleigh-Bénard convection in confined enclosures of cubic form, and mixed-convection flow over ventilated cavities. All these flows are characterized by complex dynamics of coherent structures formed in unstable flow zones. For the flow around the heated cylinder, in addition to inertial nature effects, the detached shear layers originating at the points of separation of laminar boundary layer and vortices formed in the wake have the heat prehistory of thermal exposure. The interesting features of the R-B convection in closed cells and the mixed convection in and close to ventilated cavities heated from below or from one of the side walls are the formation of global circulation, development of emerge warmed-up plumes and buoyant jets inside them.

Last time the modeling of flows is performed increasingly with the Direct Numerical Simulation, the Large Eddy Simulation or the Detached Eddy Simulation.

Visualization of time-dependent turbulent flow purposely showing up various coherent structures is not an easy problem, and the difficulties depend on the object of investigation. One of the general approaches is a proper highlighting of a vortex generation process, vortex evolution and interaction. Popular vortex-identification methods are presented in [1, 2]. As a rule, the visualization

practice of such objects is based on the vector notion. Before generation of an image, the investigator has to do the data translation into a suitable iconic representation, deciding which features in the data are meaningful for him. Three types of elementary vector icons: point, line and surface, often and often are used in flow visualization. They are based on a resemblance between the object and its representation. Lines can provide a continuous representation of the data. Line icons are drawn to show the directions and magnitudes of the flow vectors. Among of three kinds of line icons the user can choose one or another, which emphasizes different aspects of the flow. Particle trajectories generated by fluid elements over acquisition time are imitated injecting of smoke into a flow with long exposure photograph. The path is generated over several time steps and a collection of particle traces gives an image of time evolution of the flow. However the prolonged exposition leads to entangle of paths and obstruction of view on object by needless fragments. One can use combined methods – to superpose the vector field values with mapping of derived fields or showing of streamvise vorticity components and magnitude contours or tensor invariants, for example using the positive second invariant of $\nabla\mathbf{U}$, defined as Q criterion [3]: $Q = -\frac{1}{2}u_{i,j}u_{i,j} = \frac{1}{2}\left(\|\mathbf{\Omega}\|^2 - \|\mathbf{S}\|^2\right) > 0$, where the norm is $\|*\| = \sqrt{tr(*\bullet *^T)}$. It is used to find regions where the vorticity magnitude prevails over the strain-rate magnitude.

In flows induced by thermo-gradient forces the traditional technique of direct portrayal could be intensified by mapping of vector field onto non-stationary isothermal surfaces that are moving follow the gradients and that define a turbulent stirring. Below such specific flow features as large-scale circulation and turbulent plumes in the cubic cell, heated trails in and downstream of the opened-from-above cavity and vortices behind the cylinder are indicated using visualization techniques accentuated by general flow structure.

2 NUMERICAL SOLVER AND VISUALIZATION TOOL

Numerical data for turbulent flows under present consideration were obtained on the basis of the Navier-Stokes (NS) equations. Computations have been carried out using the in-house 3D code SINF [4] based on the second-order finite-volume spatial discretization, using the cell-centered variable arrangement and body-fitted block-structured grids. The code solves the conservative form of the NS equations. The ideas of the artificial compressibility method or the compressibility scaling technique are employed to compute both incompressible and compressible fluid flows. The pseudo-time evolution problem is solved using implicit schemes such as the approximate-factorization scheme or the Gauss-Seidl plane/line relaxation schemes. Dealing with unsteady flows, the pseudo-time iterations are performed for each physical time step. Three-layer second-order scheme was implemented for physical time stepping. Central and second-order upwind schemes are employed for convective flux evaluation. For low-speed flows, the solver uses a generalized Rhie-Chow interpolation to avoid de-coupling between velocity and pressure. High- and low-Reynolds number versions of several one- and two-parametric differential turbulence models are available for simulation of turbulent flows in the RANS mode. The code capabilities were extended to apply the DNS, LES and DES techniques. The algorithm discretely conserves the energy.

The code has been parallelized using MPI. The parallelization is based on the domain decomposition according to block-structuring of grids, Single Program Multiple Data strategy, and the MPI standard. The main peculiarities of parallelization concern the data exchange at the interface regions between logical neighboring subdomains. Virtual blocks were formed from near-interface

layers of connecting physical blocks, with copying all the data needed for computations of fluxes through the interface. Note that the virtual block concept adopted in the code SINF ensures the conservation of the fluxes at the interface and facilitates solution of many problems associated with the use of non-matching grids and/or with complicated conjugate heat/mass transfer tasks. In order to achieve a high efficiency of parallelization and to avoid the use of a large single master process, copies of near-interface layers of the physical blocks are created in a special process, and the latter performs the interface updating in the same manner as in the serial mode.

DNS without of whatever model of turbulence was performed to study the flows considered below. Visualization of results was performed using tools of the in-house authorized system LEONARDO. The different representation of swirled/twisted spatiotemporal objects with various levels of idealization, rendering and visibility culling were used. In particular method of filtered maps and attached vectors fields on magnitude of vorticity and temperature iso-surfaces were used for search of large scale structures in the wake behind the circular cylinder, eddy plumes in the confined cavity, eddies and heated trails in the flow inside and over the ventilated cavity.

3 CASES CONSIDERED

3.1 Flow over a heated circular cylinder

Simulation of the air flow over circular cylinder and heat transfer from its surface was performed for the Reynolds number of 5900. This case is characterized by the laminar boundary layer separation. A computational domain with the outer boundary located at 14 diameters far away from the cylinder was used. The spanwise domain size was chosen as two cylinder diameters, and periodicity conditions were imposed in this direction. The six-block grid used contained 218000 cells. The uniform velocity conditions were imposed at the inlet of the computational domain, and a constant pressure was specified at the outlet. Constant temperature (higher than at inlet) was specified on the cylinder surface.

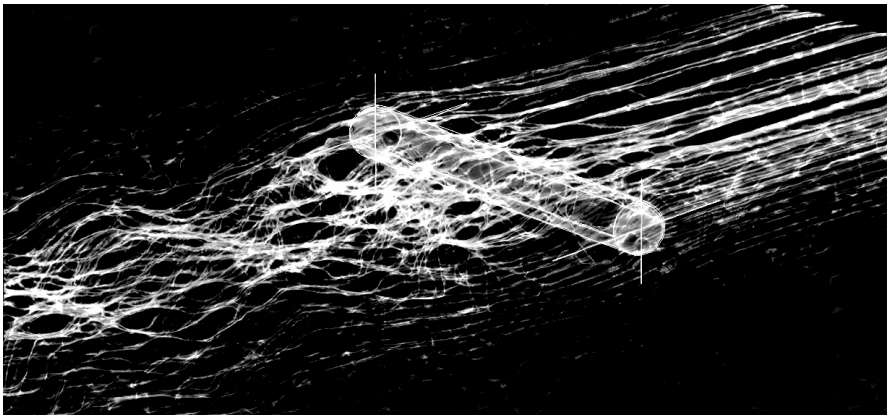

Fig. 1. Stylized stream lines for the flow over a cylinder (four times scaled along the cylinder axis)

Some results of visualization of flow structures behind the cylinder are shown on Fig. 1, 2. The flow is characterized by development of high intensive crossflow vortices (Karman vortex shedding) and their large-amplitude variations both in spanwise and downstream direction. The shown field of the vorticity vector attached to a magnitude surface gives a better representation of

the vortex structure of the flow than the conventional visualization using the standard point vectors icons.

A comparison (Fig.3) of the computed pressure coefficient distribution along the cylinder surface with experimental results [5] and the Nusselt number distributions along the cylinder surface with experimental data [6] shows a good agreement of the DNS results with measurements.

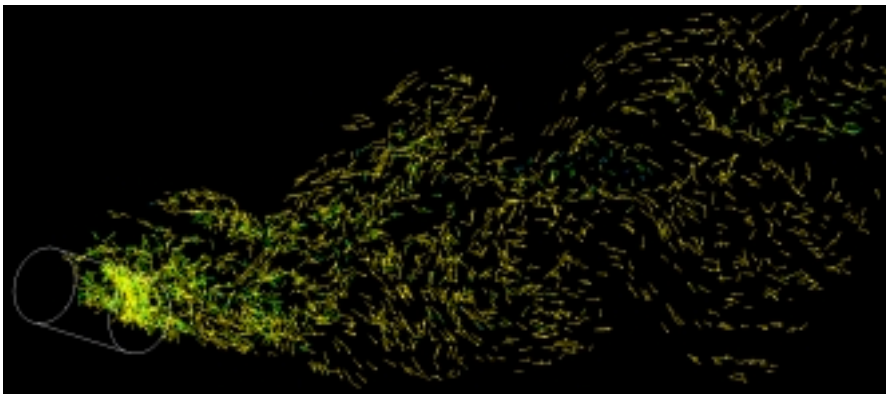

*Fig. 2. Vorticity vector field mapped onto an iso-surface of vorticity magnitude of |**rotU**|=0.8*

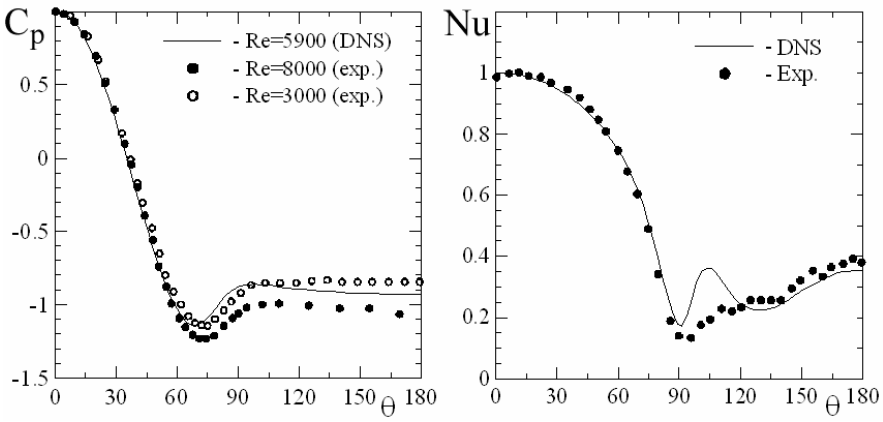

Fig. 3. Time/spanwise averaged pressure coefficient and Nusselt number distributions over the cylinder surface

Up to the time-averaged position of the boundary layer separation ($\theta \approx 85^{o}$), the local heat transfer rate computed is in a good agreement with the measured one. After the local minimum at the separation position, the behavior of the Nusselt number computed is in a proper agreement with the experiment too.

3.2 Thermal convection in a cubic enclosure

The second case under consideration is the thermal convection in a cubic cell filled with water and heated from below. The Boussinesq approximation was used to account for the buoyancy effects. The cold top and hot bottom plates are maintained at constant temperatures, and the gravity vector points downwards. The lateral walls of the cells are adiabatic. No-slip velocity boundary conditions are imposed on all the walls. With given geometry, the flow dynamics in the cells is fully determined

by values of the Prandtl number $\mathrm{Pr} = 7$, and the Rayleigh number $Ra = 5\times10^8$. The computational mesh contained $56\times56\times56$ cells.

Simulation of the turbulent RB convection in the cell reproduced clearly prominent features of such internal flow. First feature, typical for low aspect ratio tanks, consists in formation of a stable large-scale circulation that spans the whole height of the cell. Other notable feature of the convection is associated with vertical movement of thermal plumes. As shown in Fig. 4 these coherent mushroom-head structures arise from the top and bottom temperature boundary layers and move in the opposite wall direction.

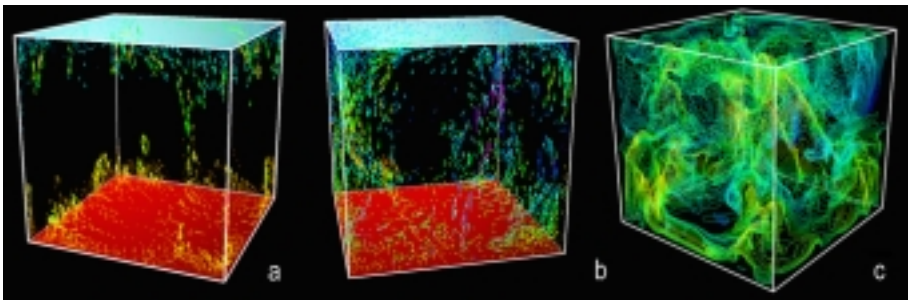

Fig. 4. Velocities vectors associated with temperature contours (a: $\theta = 0.4 - 0.6$; b: $\theta = 0.45 - 0.55$ c: iso-surface $\theta = 0.5$ mapped by contours of z-component of velocity)

Strong turbulent mixing in the flow core prevents thermals to move through the central part of the cell. As a result, most of thermals are localized near the lateral walls including regions of rising and descending large-scale motion.

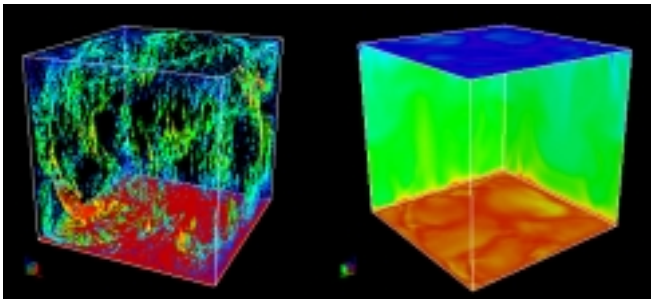

Fig. 5. Thermal jets and plumes near the cell diagonal plane and temperature fronts in the bottom boundary layer

Case monitoring of time frames of temperature field (Fig. 5) and moving of associated velocity icons made it clear that global lifting-sinking convection of flow is mostly located at different sides of the cell with respect to one of the cubic diagonal planes.

3.3 Thermal convection inside and over a row of ventilated cavity

Simulation of air mixed-convection inside and over a row of ventilated cavities with heating of the bottom or side walls was performed for Re of 10,000. The buoyancy effects were studied in a range of the Rayleigh number: $3.48\cdot10^8 \le Ra \le 13.9\cdot10^8$. For the particular configuration considered, the flow with uniform inlet velocity distribution passes over rectangular cavities periodically located along the front line. This generic case is related to some specific tasks of industrial building design. As above, the simulation was done on the basis of the NS equations using the Boussinesq

approximation to account for buoyancy effects. No-slip velocity boundary conditions are imposed on the cavity walls and the plate, and the periodicity conditions were set on corresponding boundaries. The unheated walls of the cells are adiabatic. Computational multi-block meshes used contained up to 430,000 cells.

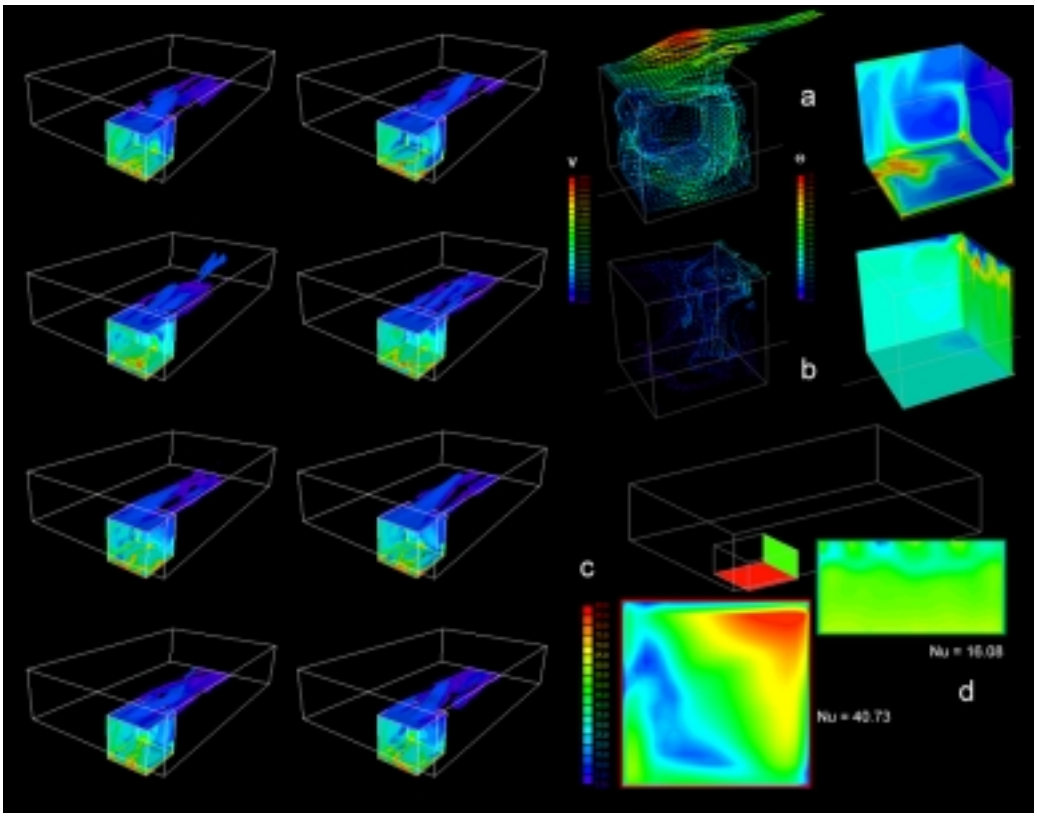

Fig. 6. Snapshots of spatial structures in flow inside and over ventilated cavity.
a - heated bottom, b – heated front windward wall.
Distribution of Nusselt number in cavity: (c)case of heated bottom and (d)case of front heated wall.

It has been established that the global air circulation inside the cavity and time-dependent vortex generation depend on the cavity wall size ratios and on the heating scheme. Time-dependent structures are induced both by shear instabilities of the detached shear layer originating at the cavity leading edge and unstable temperature stratification inside the cavity.

In cavities heated from below thermals are carried out to the main stream along cavity corners and follow a global convection circulation concentrated near a diagonal plane. Coherent vortex structures developing in a cavity depend on its configuration (cubic or parallelepiped oblong in one of the horizontal direction). Typically, two to four vortex plumes penetrate into the main stream. This process is quasi-periodic. The main vortex sheet periodically changes direction of air transfer to the left or the right edge of the cavity, and pulsation intensity of these changes is rather high. It is shown on frames of animation and is illustrated also on pictures with distributions of the vector field associated temperature (Fig. 6.).

In case of front heated walls (windward or leeward) the air circulation is not as intensive as in the previous case. Vortex generation has more local properties, and gradients of heat transfer rate are observed near upper edges of the cavity only. It adversely affects the heat transfer from the walls, the heat transfer rate decreases to two-three times as compared with the heated bottom case.

Analysis of simulation results for heat transfer obtained for cavities of various wall size ratios has shown that the highest transfer rate is observed in the heated-from-below cavity possessing the following wall size ratio: H/W/L=0.5/1/1 where H is the cavity depth. In this case the average Nusselt number was of about 40. In variants of vertical wall heating the average Nusselt number does not exceed half of this level.

4 VISUALIZATION TRICKS

Details of convection in the cell and over open cavities were investigated using different mapping and some transparent matter visualization functions with icons imitated dye streamlines and energy-diffused droplet trajectories. The nature of driving force for vortex movement was used to choose icons for representation of flow coherent structure. Mainly used variables were primitives. Derived variables were used for vortex identification. Animation of flows with turbulent fluctuations was done attracting the line/surface icons distribution attached to an appropriate matter. The development of a large-scale circulation and thermal plumes observed in numerical solutions for the R-B convection in the cubic cell was in accordance with experimental findings.

ACKNOWLEDGEMENTS

Authors would like express their thanks to Russian Foundation for Basic Research for support of the work under grant # 05-07-90038.

REFERENCES

1. Jeong J., Hussain F. On the identification of a vortex, *J. Fluid Mech.*, **285**, pp. 69-94, 1995.
2. Kida S., Miura H. Identification and analysis of vertical structures, *Eur. J. Mech. B/Fluids*, **17**, pp. 471-488, 1998.
3. Hunt J., Wray A., Moin P. Eddies, stream, and convergence zones in turbulent flows, *Center for Turbulent Research Report CTR-S88*, pp. 193-208, 1988.
4. Smirnov E.M. Recent advances in numerical simulation of 3D unsteady convection controlled by buoyancy and rotation. Keynote lecture. *CD-ROM Proc. of the 12th International Heat Transfer Conference, Grenoble, Franc, August 18-23*, 12p, 2002.
5. Yokuda S., Ramaprian B.R. The dynamics of flow around a cylinder at subcritical Reynolds numbers, *Phys. Fluids A.*, **2** (5), pp.784-791, 1990.
6. Nakamura H., Igarashi T. Unsteady heat transfer from a circular cylinder for Reynolds numbers from 3000 to 15000, In: K. Hanjalic, Y. Nagano and M. Timmers (eds.), Turbulent Heat and Mass Transfer, **4**, 2003.